NO_2-initiated multiphase oxidation of SO_2 by O_2 on $CaCO_3$ particles

Ting Yu*, Defeng Zhao*, Xiaojuan Song, Tong Zhu

BIC-ESAT and SKL-ESPC, College of Environmental Sciences and Engineering, Peking University, Beijing, 100871, China

*These authors contributed equally to this work.

Correspondence to: Tong Zhu (tzhu@pku.edu.cn)

Abstract. The reaction of SO_2 with NO_2 on the surface of aerosol particles has been suggested to be important in sulfate formation during severe air pollution episodes in China. However, we found that the direct oxidation of SO_2 by NO_2 was slow and might not be the main reason for sulfate formation in ambient air. In this study, we investigated the multiphase reaction of SO_2 with an O_2/NO_2 mixture on single $CaCO_3$ particles using Micro-Raman spectroscopy. The reaction converted the $CaCO_3$ particle to a $Ca(NO_3)_2$ droplet, with $CaSO_4 \cdot 2H_2O$ solid particles embedded in it, which constituted a significant fraction of the droplet volume at the end of the reaction. The reactive uptake coefficient of SO_2 for sulfate formation was on the order of 10^{-5}, which was higher than that for the multiphase reaction of SO_2 directly with NO_2 by 2–3 orders of magnitude. According to our observations and the literature, we found that in the multiphase reaction of SO_2 with the O_2/NO_2 mixture, O_2 was the main oxidant of SO_2 and was necessary for radical chain propagation. NO_2 acted as the initiator of radical formation, but not as the main oxidant. The synergy of NO_2 and O_2 resulted in much faster sulfate formation than the sum of the reaction rates with NO_2 and with O_2 alone. We estimated that the multiphase oxidation of SO_2 by O_2 initiated by NO_2 could be an important source of sulfate and a sink of SO_2, based on the calculated lifetime of SO_2 regarding the loss through the multiphase reaction versus the loss through the gas-phase reaction with OH radical. Parameterizing the reactive uptake coefficient of the reaction observed in our laboratory for further model simulation is needed, as well as an integrated assessment based on field observations, laboratory study results, and model simulations to evaluate the importance of the reaction in ambient air during severe air pollution episodes, especially in China.

1 Introduction

It has been suggested that multiphase or heterogeneous oxidation of SO_2 potentially plays an important role in sulfate formation in the atmosphere (Seinfeld and Pandis, 2006). During the severe pollution episodes that occur frequently in China, high sulfate concentrations cannot be explained by the gas phase oxidation of SO_2 and its well-known aqueous chemistry (Zheng et al., 2015a; Cheng et al., 2016), highlighting the role of under-appreciated heterogeneous oxidation or multiphase pathways.

Recently, the multiphase oxidation of SO_2 by NO_2 has been introduced in air quality model simulations to explain the discrepancy between the modeled and observed sulfate concentration during severe pollution episodes in China (Cheng et al., 2016; Gao et al., 2016; Wang et al., 2016; Xue et al., 2016), despite the uncertainties in the kinetic parameters for SO_2 oxidation and in the pH value of aerosol particles in China (Wang et al., 2016; Cheng et al., 2016; Liu et al., 2017; Guo et al., 2017). However, according to our recently published results (Zhao et al., 2017), the direct oxidation of SO_2 by NO_2 could not contribute significantly to sulfate formation in the atmosphere because the reactive uptake coefficient of SO_2 for sulfate formation due to direct oxidation by NO_2 is very low (~10^{-8}).

Although the contribution of the direct oxidation of SO_2 by NO_2 to sulfate formation is not significant, NO_2 may be involved in other oxidation pathways of SO_2. It has been reported that the reaction of NO_2 with SO_3^{2-} and HSO_3^- in the bulk aqueous phase can form the $SO_3^{\bullet-}$ radical, which can further react with O_2 and produce a series of radicals that oxidize S(IV) species (Littlejohn et al., 1993). The reaction pathway may result in a fast SO_2 oxidation due to the potential synergy of NO_2 and O_2.

Despite such a reaction mechanism for SO_2 oxidation being proposed, its role in SO_2 oxidation in the ambient atmosphere is not well established. Most previous studies have focused on the direct reaction of SO_2 with NO_2, including the determination of its rate constant (Lee and Schwartz, 1983; Clifton et al., 1988; Shen and Rochelle, 1998; Spindler et al., 2003; Nash, 1979; Huie and Neta, 1986). According to the reaction products and their reported yields (Lee and Schwartz, 1983; Clifton et al., 1988), the overall reaction equations of the direct reaction of SO_2 with NO_2 are as follows:

$$2NO_2(aq) + HSO_3^-(aq) + H_2O \rightarrow 2NO_2^-(aq) + SO_4^{2-}(aq) + 3H^+(aq), \quad \text{(R1)}$$

$$2NO_2(aq) + SO_3^{2-}(aq) + H_2O \rightarrow 2NO_2^-(aq) + SO_4^{2-}(aq) + 2H^+(aq), \quad \text{(R2)}$$

and the reactions are proposed to proceed via NO_2–S(IV) adduct complexes (Clifton et al., 1988).

$$NO_2(aq) + SO_3^{2-}(aq) \rightarrow [NO_2 - SO_3]^{2-}(aq). \quad \text{(R3)}$$

$$NO_2(aq) + [NO_2 - SO_3]^{2-}(aq) \rightarrow [NO_2 - SO_3 - NO_2]^{2-}(aq). \quad \text{(R4)}$$

$$[NO_2 - SO_3 - NO_2]^{2-}(aq) + OH^-(aq) \rightarrow [NO_2 - SO_4H - NO_2]^{3-}(aq). \quad \text{(R5)}$$

$$[NO_2 - SO_4H - NO_2]^{3-}(aq) \rightarrow 2NO_2^-(aq) + SO_4^{2-}(aq) + H^+(aq). \quad \text{(R6)}$$

Additionally, NO_2–S(IV) adduct complex may decompose as follows (Spindler et al., 2003).

$$[NO_2 - SO_3]^{2-}(aq) \rightarrow NO_2^-(aq) + SO_3^{\bullet-}(aq). \quad \text{(R7)}$$

However, studies of the oxidation rate of SO_2 at the O_2 concentrations relevant to the ambient atmosphere and the potential influence of the synergy of NO_2 and O_2 on the oxidation rate are very limited (Turšič et al., 2001; He et al., 2014), except a few studies investigated SO_2 oxidation in the presence of NO_2 as well as O_2 (Littlejohn et al., 1993; Shen and Rochelle, 1998; Santachiara et al., 1990). Moreover, previous studies have mainly focused on the

reaction in bulk solution and only few studies have investigated the oxidation of SO_2 by NO_2 on aerosol particles (Santachiara et al., 1990, 1993). On aerosol particles, water activity, pH, ionic strength, the presence of other compounds or ions, and the role of particle surface are different from in dilute bulk solution and may affect the reaction process and reaction rate. Therefore, further studies of the multiphase reaction of SO_2 with O_2/NO_2 mixtures on aerosol particles are required to determine the kinetic parameters and the mechanism of the reaction.

In this study, we investigated the multiphase reaction of SO_2 with O_2 in the presence of NO_2 on $CaCO_3$ particles. We quantified the reactive uptake coefficient of SO_2 due to the reaction with an $O_2/NO_2/H_2O$ mixture. Based on our observations and the existing literature, we further discussed the reaction mechanism. Furthermore, we estimated the role of the multiphase oxidation of SO_2 by O_2 in the presence of NO_2 in the atmosphere.

2 Experimental

The experiments were conducted using a flow reaction system and the setup is shown in Fig. S1. The experimental setup and procedure used have been described in detail in previous studies (Zhao et al., 2017; Zhao et al., 2011; Liu et al., 2008). A gas mixture of NO_2, SO_2, O_2, N_2, and water vapor reacted with particles deposited on a substrate in the flow reaction cell. The concentrations of SO_2 and NO_2 were controlled using mass flow controllers by varying the flow rates of SO_2 (2,000 ppm in high purity N_2, National Institute of Metrology P.R. China), NO_2 (1,000 ppm in high purity N_2, Messer, Germany), and synthetic air [20% O_2 (high purity grade: 99.999%, Beijing Haikeyuanchang Practical Gas Co., Ltd.) and 80% N_2 (high purity grade: 99.999%, Beijing Haikeyuanchang Practical Gas Co., Ltd.)]. Relative humidity (RH) was controlled by regulating the flow rates of reactant gases, dry synthetic air, and humidified synthetic air. Humidified synthetic air was prepared by bubbling synthetic air through fritted glass in water. In some experiments, the O_2 concentrations were varied by regulating the mixing ratios of O_2 and N_2 to investigate the effect of O_2. $SO_2/O_2/NO_2/H_2O$ mixtures flew through the reaction cell and reacted with individual stationary $CaCO_3$ particles, which were deposited on a Teflon-FEP film substrate annealed to a silicon wafer. RH and temperature were measured using a hygrometer (HMT100, Vaisala, Vantaa, Finland) at the exit of the reaction cell. Additionally, temperature was measured using another small temperature sensor (Pt 100, 1/3 DIN B, Heraeus, Hanau, Germany) in the reaction cell. All the experiments were conducted at 298 ± 0.5 K. The experiments were conducted under two RHs (72% and 82%) at 75 ppm SO_2 and 75 ppm NO_2.

During the reaction, particles were monitored *in-situ* via a glass window on the top of the reaction cell using a Micro-Raman spectrometer (LabRam HR800, HORIBA Jobin Yvon, Kyoto, Japan) to obtain microscopic images and Raman spectra. A 514-nm excitation laser was used, and back scattering Raman signals were detected. The details of the instrument are described elsewhere (Liu et al., 2008; Zhao et al., 2011). Because the particles were larger than the laser spot in this study (~1.5 μm), confocal Raman mapping was used to measure the spectra at different locations on a particle to obtain the chemical information of the entire particle. The mapping area was rectangular and was slightly larger than the particle, with mapping steps of 1 × 1 μm. Raman spectra in the range of 800–3,900 cm^{-1} were acquired with an exposure time of 1 s for each mapping point. Raman spectra were analyzed using Labspec 5 software (HORIBA Jobin Yvon). Raman peaks were fitted to Gaussian–Lorentzian

functions to obtain peak positions and peak areas at different locations on the particle. The peak areas were then added together to obtain the peak area for the entire particle.

Particles of $CaCO_3$ (98%, Sigma-Aldrich, USA), with average diameters of about 7–10 μm as specified by the supplier, were used in the experiments. The $CaCO_3$ particles were rhombohedron crystals; X-ray diffraction analysis indicated that they were calcite (Fig. S2). Individual particles were prepared by dripping a dilute $CaCO_3$ suspended solution onto Teflon-FEP film using a pipette and then drying the sample in an oven at 80ºC for 10 h.

The amount of $CaSO_4$ as a reaction product was quantified based on Raman peak areas and particle sizes. The details of the method are described in our previous study (Zhao et al., 2017). Briefly, the amount of reaction product $CaSO_4$ formed was determined as a function of time using Raman peak areas. Raman peak areas were converted to the amount of compound formed using a calibration curve obtained from pure $CaSO_4$ particles of different sizes, which were determined according to microscopic images. The reaction rate, i.e., the sulfate production rate, was derived from the amount of sulfate formed as a function of time. The reactive uptake coefficient of SO_2 for sulfate formation (γ) was further determined from the reaction rate and collision rate of SO_2 on the surface of a single particle.

$$\gamma = \frac{\frac{d\{SO_4^{2-}\}}{dt}}{Z} \quad . \tag{1}$$

$$Z = \frac{1}{4} c A_s [SO_2], \tag{2}$$

$$c = \sqrt{\frac{8RT}{\pi M_{SO_2}}} \quad , \tag{3}$$

where R is the gas constant, T is temperature, Mso_2 is the molecular weight of SO_2, c is the mean molecular velocity of SO_2, A_s is the surface area of an individual particle, and Z is the collision rate of SO_2 on the surface of a particle. $\{SO_4^{2-}\}$ indicates the amount of sulfate in the particle phase in moles. The average reaction rate and surface area of particles during the multiphase reaction period were used to derive the reactive uptake coefficient. The period was chosen to start after the induction period when ~10% of the final sulfate was formed. $[SO_2]$ indicates the concentration of SO_2 in the gas phase.

The influence of gas phase diffusion on reactive uptake was evaluated using the resistor model described by Davidovits et al. (2006) and references therein, as well as using the gas phase diffusion correction factor for a reactive uptake coefficient according to the method described by Pöschl et al. (2007). The reactive uptake of SO_2 was found to not be limited by gas phase diffusion (see details in the Supplement S1).

In addition, we conducted experiments of the reaction SO_2 with only O_2 on both $CaCO_3$ solid particles and internally mixed $CaCO_3/Ca(NO_3)_2$ particles (with $CaCO_3$ embedded in $Ca(NO_3)_2$ droplets), while keeping other conditions the same as the reaction of SO_2 with an O_2/NO_2 mixture. These experiments of the multiphase oxidation of SO_2 by O_2 can help determine the role of NO_2 in the reaction of SO_2 with an O_2/NO_2 mixture.

3 Results and discussion

3.1 Reaction products and changes in particle morphology

Figure 1 shows the Raman spectra of a $CaCO_3$ particle during the multiphase reaction of SO_2 with $O_2/NO_2/H_2O$ on its surface. The peak at 1,087 cm^{-1} was assigned to the symmetric stretching of carbonate ($\nu_s(CO_3^{2-})$)

(Nakamoto, 1997). During the reaction, the peak at 1,087 cm^{-1} decreased continuously and finally disappeared as new peaks were observed. The peak at 1,050 cm^{-1} was assigned to the symmetric stretching of nitrate ($\nu_s(NO_3^-)$). The peaks at 1,010 cm^{-1} and 1,136 cm^{-1} were assigned to the symmetric stretching ($\nu_s(SO_4^{2-})$) and asymmetric stretching($\nu_{as}(SO_4^{2-})$) of sulfate in gypsum ($CaSO_4 \cdot 2H_2O$), respectively (Sarma et al., 1998). In addition, after the reaction, a broad envelope in the range of 2,800–3,800 cm^{-1} assigned to the stretching of the OH bond in water molecules was observed. Above this envelope, there were two peaks at 3,408 cm^{-1} and 3,497 cm^{-1}, which were assigned to OH bond stretching in crystallization water of $CaSO_4 \cdot 2H_2O$ (Sarma et al., 1998; Ma et al., 2013).

During the multiphase reaction with the $SO_2/O_2/NO_2/H_2O$ mixture, the $CaCO_3$ particles displayed a remarkable change in morphology. The original $CaCO_3$ particle was a rhombohedron crystal (Fig. 2, panel i, a). As the reaction proceeded, its edges became smoother and later a transparent droplet layer formed, which had a newly formed solid phase embed in it (Fig. 2, panel i, d). The size of the new solid phase grew during the reaction (Fig. 2, panel i, d–f) and it seemed to contain many micro-crystals. Raman mapping revealed that the new solid phase consisted of $CaSO_4 \cdot 2H_2O$ (Fig. 2, panel iv), and the surrounding aqueous layer consisted of $Ca(NO_3)_2$ (Fig. 2, panel iii).

The particle morphology change shown in Fig. 2 was significantly different from the morphology change in the direct reaction of SO_2 with NO_2 (Zhao et al., 2017), where the $CaCO_3$ particle was first converted to a spherical $Ca(NO_3)_2$ droplet and then needle-shaped $CaSO_4$ crystals formed inside the droplet (Zhao et al., 2017). Moreover, the amount of $CaSO_4$ formed in this study was much higher than that in the direct reaction of SO_2 with NO_2. The $CaSO_4$ solid particle constituted a significant fraction of the volume of the droplet, while in the direct reaction of SO_2 with NO_2 the few needle-shaped $CaSO_4$ crystals that formed only constituted a small fraction of the droplet volume (Zhao et al., 2017).

3.2 Reaction process

During the reaction, the amounts of carbonate, nitrate, and sulfate were determined as a function of time, as shown in Fig. 3. At the beginning of the reaction, the amount of carbonate decreased slowly, while the amount of nitrate and sulfate increased slowly. After a period of induction of around 50 min, the reaction accelerated significantly, leading to a rapid consumption of carbonate and production of nitrate and sulfate. The decrease in the amount of carbonate and the increase in the amount of nitrate was because carbonate reacted continuously with NO_2 and H_2O, forming $Ca(NO_3)_2$. The detailed mechanism of the multiphase reaction of carbonate with NO_2 and H_2O were discussed in our previous studies (Li et al., 2010; Zhao et al., 2017). The mechanism of sulfate formation is discussed in detail in Section 3.4 of the present study. Finally, the carbonate was completely consumed, and the amounts of nitrate and sulfate levelled off.

Figure 3 shows that nitrate and sulfate were formed simultaneously during the reaction. This contrasts with the observations made during the direct reaction of SO_2 with NO_2, where nitrate was formed first, and sulfate was essentially formed after the complete conversion of $CaCO_3$ particles to $Ca(NO_3)_2$ droplets (Zhao et al., 2017). Moreover, the time taken for carbonate to be completely consumed was longer in this study than in the direct reaction of SO_2 with NO_2 (~120 vs. ~40 min) when other conditions were kept the same (Zhao et al., 2017).

3.3 Reactive uptake coefficient of SO_2

The reactive uptake coefficients of SO_2 for sulfate formation (γ) in the reaction of SO_2 with the $O_2/NO_2/H_2O/N_2$ mixture on $CaCO_3$ with various O_2 concentrations are shown in Table 1. The value of γ for the reaction of SO_2 with O_2/NO_2 at three O_2 concentrations (5, 20, and 86%) was in the range of $(0.35–1.7) \times 10^{-5}$, and was 1.2×10^{-5} in synthetic air. This latter value was 2–3 orders of magnitude higher than that for the reaction of SO_2 directly with NO_2 under similar conditions (Zhao et al., 2017). When other conditions were kept constant, γ increased with the O_2 concentration. This indicates that O_2 played a key role in enhancing the oxidation rate of SO_2.

The role of O_2 in enhancing the reactive uptake of SO_2 reported here is consistent with the findings in some previous studies. For example, Littlejohn et al. (1993)'s data showed that sulfite oxidation rate increases with the O_2 concentration (0–5% by volume). Shen and Rochelle (1998) also found that in the presence of O_2, the aqueous sulfite oxidation rate is enhanced. By investigating the oxidation of SO_2 by NO_2 in monodispersed water droplets growing on carbon nuclei, Santachiara et al. (1990) found that sulfate formation rate with 2% O_2 is much higher than that without O_2. Yet, our findings, as well as those in the studies referred to above, are in contrast to those reported by Lee and Schwartz (1983), who found that changing from N_2 to air as a carrier gas only increases bisulfite oxidation rate by no more than 10%. The difference between our study and Lee and Schwartz (1983) could be due to the difference in O_2 diffusion from gas to the condensed phase and the different mechanisms between the multiphase reaction on particles and the aqueous reaction.

Only few studies have reported the S(IV) oxidation rate in the reaction of S(IV) with O_2/NO_2 mixtures (Turšič et al., 2001; Littlejohn et al., 1993). However, due to the limiting step by the aqueous phase mass transfer, it is difficult to quantitatively compare the reaction rates in those studies with the uptake coefficient in our study and the rate constants determined by Lee and Schwartz (1983) and Clifton et al. (1988). For example, a rate constant of 2.4×10^3 mol^{-1} L s^{-1} (at pH 3) can be derived from the results of Turšič et al. (2001), which is much lower than the values reported by Lee and Schwartz (1983) and Clifton et al. (1988). This can be attributed to the limiting step by the aqueous-phase mass transfer because the characteristic mixing time in the aqueous phase in Turšič et al. (2001) was likely much longer than that of Lee and Schwartz (1983) (1.7–5.3 s), according to the HSO_3^- concentration time series reported by Turšič et al. (2001).

It is important to note that the concentrations of NO_2 and SO_2 used in this study are much higher than those in the ambient atmosphere. High concentrations of reactant gases are often used in laboratory studies in order to simulate the ambient reactions at the time scale of days or weeks and to get high signal-to-noise ratios for detecting products within minutes or hours. In the ambient atmosphere, reactive uptake coefficient of SO_2 should be lower than that in this study due to the lower NO_2 concentrations when other conditions are comparable and the chemical/physical processes observed in this study, such as changes in particle composition, phase, hygroscopicity, and pH should be much slower due to the lower concentrations of NO_2 and SO_2.

3.4 Reaction mechanism

In the multiphase reaction of SO_2 with $O_2/NO_2/H_2O$ on $CaCO_3$ particles, we found that $CaCO_3$ reacted with NO_2 and H_2O and produced $Ca(NO_3)_2$, which deliquesced, forming liquid water, and provided a site for the

aqueous oxidation of SO_2. This process is similar to the direct reaction of SO_2 with NO_2 on $CaCO_3$ particles. The details of this part of the reaction mechanism were discussed in our previous study (Zhao et al., 2017).

Once the aqueous phase was formed, SO_2 could undergo multiphase reactions with O_2/NO_2. The mechanism of the direct aqueous reaction of S(IV) with NO_2 in the absence of O_2 is complex. Previous studies have proposed two different mechanisms for the reaction. One involves $SO_3^{\bullet-}$ radical formation (Littlejohn et al., 1993; Shen and Rochelle, 1998; Turšič et al., 2001) (referred as "free-radical chain" mechanism, while the other involves the formation of NO_2–S(IV) complexes (Clifton et al., 1988), but no radical formation (referred as "NO_2–S(IV) complex" mechanism).

According to the NO_2–S(IV) complex mechanism, the presence of O_2 should not affect the SO_2 oxidation rate; however, in this study, a substantial enhancement in the SO_2 oxidation rate was observed in the presence of O_2 compared with that in the absence of O_2. Therefore, the NO_2–S(IV) complex mechanism was less likely to have been important in this study.

In the free-radical chain mechanism, the $SO_3^{\bullet-}$ radical is proposed to be formed (R8, Table 2), which is based on the observation of $S_2O_6^{2-}$ formation, with $S_2O_6^{2-}$ known to be the combination reaction product of $SO_3^{\bullet-}$ (Eriksen, 1974; Hayon et al., 1972; Deister and Warneck, 1990; Brandt et al., 1994; Waygood and McElroy, 1992). In addition to SO_4^{2-} and NO_2^-, $S_2O_6^{2-}$ was detected with an appreciable yield using Raman spectroscopy, following the reaction of NO_2 with aqueous sulfite (Littlejohn et al., 1993). $S_2O_6^{2-}$ was also observed in the aqueous oxidation of bisulfite in an N_2-saturated solution in the presence of Fe(III) using ion-interaction chromatography (Podkrajšek et al., 2002). The $SO_3^{\bullet-}$ radical can react via two pathways, forming either $S_2O_6^{2-}$ or SO_4^{2-} (R9–R11, Table 2). The reactions R9–R11 have been well established in studies of S(IV) oxidation by other pathways, including OH oxidation, photo-oxidation, and transition metal catalyzed oxidation (Eriksen, 1974; Hayon et al., 1972; Deister and Warneck, 1990; Brandt et al., 1994; Brandt and Vaneldik, 1995; Waygood and McElroy, 1992). In addition, although previous studies have not reported the direct observation of the $SO_3^{\bullet-}$ radical in the aqueous reaction of S(IV) with NO_2, $SO_3^{\bullet-}$ was observed in the reaction of NO_2^- with SO_3^{2-} in an acidic buffer solution (pH = 4.0) using electron spin resonance (ESR) (Shi, 1994). Because NO_2^- is formed in the aqueous reaction of SO_2 with NO_2, and $S_2O_6^{2-}$ as the combination reaction product of $SO_3^{\bullet-}$ is observed (Littlejohn et al., 1993), $SO_3^{\bullet-}$ formation is plausible.

In the presence of O_2, the $SO_3^{\bullet-}$ radical can react rapidly with O_2, forming the $SO_5^{\bullet-}$ radical (R12, Table 2). Following this reaction, a number of chain reactions can occur to ultimately form sulfate (Littlejohn et al., 1993; Seinfeld and Pandis, 2006; Shen and Rochelle, 1998) (R13–R16, Table 2). Littlejohn et al. (1993) observed that the amount of $S_2O_6^{2-}$ relative to SO_4^{2-} formed in the aqueous reaction of NO_2 with sulfite decreases in the presence of O_2 compared with the reaction in the absence of O_2. At low NO_2 concentrations (< 5 ppm), $S_2O_6^{2-}$ is undetectable in the presence of O_2. This indicates that O_2 suppresses the reaction pathway of $S_2O_6^{2-}$ formation (R9, Table 2). Because the $SO_3^{\bullet-}$ radical can react rapidly with O_2, forming the $SO_5^{\bullet-}$ radical, and would therefore be consumed, the suppression of $S_2O_6^{2-}$ formation can be attributed to the reaction of $SO_3^{\bullet-}$ with O_2 (R12, Table 2). The reactions R12–R16 have been well established by studies of the oxidation of S(IV) by OH or photo-oxidation, and all the radicals have been observed (Hayon et al., 1972; Huie et al., 1989; Huie and Neta, 1987; Chameides and Davis, 1982; Seinfeld and Pandis, 2006).

The free-radical chain mechanism is consistent with the findings of this study and is therefore more plausible. The enhancement of the SO_2 oxidation rate in the reaction of SO_2 with $O_2/NO_2/H_2O$ on $CaCO_3$ particles compared with that in the direct reaction of SO_2 with NO_2/H_2O was attributed to O_2. Although during the reaction in the absence of O_2—i.e., the direct oxidation of SO_2 by NO_2—the $SO_3^{\bullet-}$ radical can be formed (R7), the reaction chain cannot propagate (R12–R16). Therefore, the S(IV) oxidation rate and the reactive uptake coefficient of SO_2 were much lower than that in the presence of O_2. According to the difference between the reactive uptake coefficient in this study and in the direct reaction of SO_2 with NO_2 (Zhao et al., 2017), the sulfate production rate via chain reactions due to the presence of O_2 (20%) was 2–3 orders of magnitude faster than the direct oxidation of SO_2 by NO_2. This indicates that sulfate production in the reaction of SO_2 with O_2/NO_2 was largely due to O_2 oxidation via the chain reaction pathway, i.e., "autoxidation" of S(IV), rather than the direct oxidation of SO_2 by NO_2 and thus O_2 was the main oxidant of SO_2.

In addition to the two mechanisms above, Spindler et al. (2003) proposed a reaction mechanism involving first NO_2–S(IV) complex formation and subsequent $SO_3^{\bullet-}$ radical formation (R3, R7). NO_2–S(IV) complex may establish an equilibrium with $SO_3^{\bullet-}$ in contrast to the direct formation of $SO_3^{\bullet-}$ via the reaction of NO_2 with SO_2. Higher concentration of O_2 favors the conversion of $SO_3^{\bullet-}$ to $SO_5^{\bullet-}$ and thus can reduce the $SO_3^{\bullet-}$ concentration, shifting the equilibrium to the product side and promoting the overall S(IV) oxidation. O_2 can act in a similar way as in the free-radical chain mechanism. Admittedly, we cannot rule out the possibility NO_2–S(IV) complex formation. But such a mechanism can still be classified as the free-radical chain mechanism since the S(IV) oxidation still proceeds via the radical chain reactions.Although the direct oxidation of SO_2 by NO_2 only accounted for a very small fraction of sulfate formation, NO_2 played an important role in the SO_2 oxidation by initiating the chain reactions via the production of the $SO_3^{\bullet-}$ radical (R7). In the experiment without NO_2, but with other reaction conditions the same, we were unable to detect sulfate after 5 h of reaction. This indicates that O_2 by itself cannot initiate the chain reactions (although it favors chain propagation), and that the oxidation of SO_2 by O_2 was slow. The effect on the SO_2 oxidation rate when both NO_2 and O_2 were present was much higher than the sum of the effect of NO_2 and O_2. We refer to this effect as the synergy of NO_2 and O_2, which resulted in the fast oxidation of SO_2 to form sulfate in this study. This effect is similar to a "ternary" reaction found with the reaction of NO_2–particles–H_2O or SO_2–particles–O_3 (Zhu et al., 2011), where the reaction rate can be much faster than the sum of the reaction rates for the reaction of the second and third reactant with the first reactant. In addition to acting as the initiator of chain reactions, NO_2 also contributed to the formation of the aqueous phase through the reaction with $CaCO_3$, forming $Ca(NO_3)_2$ as discussed above, which provided a site for S(IV) oxidation.

Based on the discussion above, we summarize the reaction mechanism that occurred in this study in Table 2. The reactions are classified as chain initiation, chain propagation, and chain termination. The dominant S(IV) species depends on pH. Due to the fast dissociations of $SO_2{\bullet}H_2O$ and HSO_3^-, reactions consuming one of these S(IV) species will result in instantaneous re-establishment of the equilibria between them (Seinfeld and Pandis, 2006). In this study, the pH of the aqueous layer of $Ca(NO_3)_2$ may change dynamically with time during the reaction and may not be completely homogeneous within the aqueous droplet. The pH values could vary between ~3 and ~7.6. In the surface of the aqueous layer, pH was mainly determined by the gas–aqueous equilibrium of SO_2, and was estimated to be ~3. In the vicinity of the $CaCO_3$ core, pH was mainly determined by the hydrolysis of carbonate and was estimated to be ~7.6. It is likely that both HSO_3^- and SO_3^{2-} were present, and the dominant

species depended on the reaction time and location within the aqueous droplet. Nevertheless, to make the reaction mechanism clearer, HSO_3^- was used in the reaction equations. Similar reaction equations are also applicable to SO_3^{2-} because of the fast dissociations of $SO_2 \bullet H_2O$ and HSO_3^-. Overall, the reaction can be written as follows, which clearly shows that O_2 was the main oxidant for sulfate formation:

$$2NO_2(aq) + 2HSO_3^-(aq) + (0/1)O_2 \rightarrow 2NO_2^-(aq) + S_2O_{6/8}^{2-}(aq) + 2H^+(aq), \quad \text{(R19)}$$

$$nO_2 + 2nHSO_3^-(aq) \rightarrow 2nSO_4^{2-}(aq) + 2nH^+(aq), \quad \text{(R20)}$$

where n >> 1. Once sulfuric acid was formed, it reacted with $CaCO_3$, forming $CaSO_4$:

$$CaCO_3(s) + SO_4^{2-}(aq) + 2H^+(aq) + H_2O(aq) \rightarrow CaSO_4 \bullet 2H_2O(s) + CO_2(g). \quad \text{(R21)}$$

As mentioned above, compared with the direct reaction of SO_2 with NO_2, $CaCO_3$ was consumed more slowly in the reaction with O_2/NO_2. There were two possible reasons for this. First, the $CaSO_4 \bullet 2H_2O$ formed in the reaction could cover the $CaCO_3$ surface and partly suppress the diffusion of aqueous ions, such as protons, and also limit the contact of reactants with the surface of the $CaCO_3$ particles, thus reducing the $CaCO_3$ consumption rate. Second, compared with the direct reaction of SO_2 with NO_2, a much higher fraction of $CaCO_3$ was converted to $CaSO_4 \bullet 2H_2O$ instead of $Ca(NO_3)_2$ due to the fast production of $CaSO_4 \bullet 2H_2O$. Therefore, the volume of a $Ca(NO_3)_2$ droplet was much smaller than that in the direct reaction of SO_2 with NO_2 for a given $CaCO_3$ particle. Because the uptake rate of NO_2 was proportional to the droplet surface area and the NO_2 hydrolysis rate was proportional to the droplet volume, the rate of nitric acid production from NO_2 hydrolysis and its reaction rate with $CaCO_3$ were reduced. Therefore, the $CaCO_3$ particles were consumed more slowly in the reaction with O_2/NO_2.

4 Conclusion and implications

We investigated the multiphase reaction of SO_2 with $O_2/NO_2/H_2O$ on $CaCO_3$ particles. The reaction converted $CaCO_3$ particles to $Ca(NO_3)_2$ droplets, in which $CaSO_4 \bullet 2H_2O$ was embedded and accounted for a significant fraction of the droplet volume by the end of the reaction. The $Ca(NO_3)_2$ droplet formed by the reaction of $CaCO_3$ with NO_2 provided a site for the multiphase oxidation of SO_2. Generally, nitrate and sulfate were formed simultaneously. The reactive uptake coefficient of SO_2 for sulfate formation in the reaction of SO_2 with NO_2/H_2O in synthetic air was determined to be around 10^{-5}. Compared with the reaction of SO_2 with NO_2 on a $CaCO_3$ particle in the absence of O_2, i.e., the direct oxidation of SO_2 by NO_2 in N_2, sulfate production rate in the reaction of SO_2 with O_2/NO_2 was enhanced by 2–3 orders of magnitude. According to the findings of this study and the existing literature, SO_2 oxidation likely proceeded via a free-radical chain reaction mechanism. O_2 was the main oxidant of SO_2, and NO_2 mainly acted as an initiator of the chain reactions. The synergy of NO_2 and O_2 resulted in the fast oxidation of SO_2. The absence of either NO_2 or O_2 led to much slower SO_2 oxidation.

Using a method developed in our previous study (Zhao et al., 2017), we assessed the importance of the multiphase oxidation of SO_2 by O_2 in the presence of NO_2 by estimating the lifetime of SO_2 due to multiphase reactions and the lifetime due to the gas phase reaction (with the OH radical). The lifetime of SO_2 due to the multiphase reaction of SO_2 with O_2/NO_2 was estimated to be around 20 days using the reactive uptake coefficient of SO_2 (1.2×10^{-5}) and the typical particle surface area concentration for mineral aerosols in winter in Beijing (6.3×10^{-6} cm^2 cm^{-3}) (Huang et al., 2015). This lifetime is comparable to the lifetime of SO_2 due to the gas phase

reaction with OH, which is ~12 days assuming that the daytime OH concentration is 1×10^6 molecules cm^{-3} (Lelieveld et al., 2016; Prinn et al., 2005). Therefore, we conclude that the multiphase oxidation of SO_2 by O_2 in the presence of NO_2 is likely to be an important source of sulfate and a sink of SO_2 in the ambient atmosphere, and can play a significant role in the sulfate formation during severe haze episodes, such as those that frequently occur in China. During haze episodes, there are high concentrations of SO_2 and NO_2 and relative humidity is often high (Zhang et al., 2014; Wang et al., 2016; Zheng et al., 2015b). Under these conditions, the multiphase oxidation of SO_2 by O_2 in the presence of NO_2 could proceed rapidly, forming sulfate. The enhanced sulfate concentration due to multiphase reactions and resulting aerosol water content can further promote the multiphase oxidation of SO_2. The reaction thus proceeds in a self-accelerating way. Therefore, it can contribute significantly to sulfate formation during haze episodes, which could explain the discrepancies between the observed and modelled sulfate concentrations (Cheng et al., 2016; Gao et al., 2016; Wang et al., 2016; Zheng et al., 2015a).

In addition, elucidating the mechanism of the multiphase reaction of SO_2 with $O_2/NO_2/H_2O$ in the atmosphere is important for the other atmospheric implications of the reaction besides sulfate formation. According to the reaction mechanism, the direct oxidation of SO_2 by NO_2 forms sulfate and nitrite, with a stoichiometry of 1:1, and nitrite can further form HONO under acidic conditions. The HONO could then evaporate into the atmosphere, where it would be an important source of OH radical. If NO_2 were the main oxidant of SO_2 in the multiphase reaction, the reaction would form one HONO molecule for every sulfate formed. Thus, the oxidation of SO_2 by NO_2 can simultaneously be an important source of HONO and OH radical, and SO_2 oxidation would be strongly coupled with reactive nitrogen chemistry. However, according to the mechanism of this study, NO_2 only acted as an initiator of the chain reactions in SO_2 oxidation and essentially all the SO_2 was oxidized by O_2. Therefore, the amount of HONO formation per sulfate formed was trivial. The oxidation of SO_2 by O_2/NO_2 is expected to be neither an important source of HONO and OH in the atmosphere nor to have a significant influence on reactive nitrogen chemistry.

In this study, we investigated the reaction of SO_2 with O_2 in the presence of NO_2 at three O_2 concentrations. The influence of the O_2 concentration was shown to be significant. Future experimental results with more O_2 concentration levels would provide more insights into the reaction mechanism and process.

In addition, in the ambient atmosphere, the internal mixing of organics with S(IV) in particles may influence the S(IV) oxidation rate by O_2 in the presence of NO_2. When organics is abundant in particles, for example during haze episodes in China, it can react with and thus scavenge radical anion carriers such as $SO_5^{\bullet-}$ and $SO_4^{\bullet-}$ (Herrmann, 2003; Herrmann et al., 2015; Huie, 1995). Therefore, the presence of internally mixed organics can reduce the effectivity of the potential radical reaction chain and of S(IV) oxidation, which can undermine the importance of the oxidation by O_2 in the presence of NO_2 in the overall S(IV) oxidation.

Acknowledgements

This work was supported by Natural Science Foundation Committee of China (41421064, 21190051, 40490265, 91544000) and Ministry of Science and Technology (Grant No. 2002CB410802).

References

Brandt, C., Fabian, I., and Vaneldik, R.: Kinetics and mechanism of the iron(III)-catalyzed autoxidation of sulfur(IV) oxides in aqueous-solution - evidence for the redox cycling of iron in the presence of oxygen and modeling of the overall reaction-mechanism, Inorg. Chem. , 33, 687-701, 10.1021/ic00082a012, 1994.

Brandt, C., and Vaneldik, R.: Transition metal-catalyzed oxidation of sulfur (IV) oxides. Atmospheric-relevant processes and mechanisms, Chem. Rev., 95, 119-190, 10.1021/cr00033a006, 1995.

Chameides, W. L., and Davis, D. D.: The free-radical chemistry of cloud droplets and its impact upon the composition of rain, J. Geophys. Res.-Oceans, 87, 4863-4877, 10.1029/JC087iC07p04863, 1982.

Cheng, Y. F., Zheng, G. J., Wei, C., Mu, Q., Zheng, B., Wang, Z. B., Gao, M., Zhang, Q., He, K. B., Carmichael, G., Poschl, U., and Su, H.: Reactive nitrogen chemistry in aerosol water as a source of sulfate during haze events in China, Sci. Adv., 2, 10.1126/sciadv.1601530, 2016.

Clifton, C. L., Altstein, N., and Huie, R. E.: Rate-constant for the reaction of NO_2 with sulfur(IV) over the pH range 5.3-13, Environ. Sci. Technol., 22, 586-589, 10.1021/es00170a018, 1988.

Davidovits, P., Kolb, C. E., Williams, L. R., Jayne, J. T., and Worsnop, D. R.: Mass accommodation and chemical reactions at gas-liquid interfaces, Chem. Rev., 106, 1323-1354, 10.1021/cr040366k, 2006.

Deister, U., and Warneck, P.: Photooxidation of sulfite (SO32-) in aqueous solution, J. Phys. Chem., 94, 2191-2198, 10.1021/j100368a084, 1990.

Eriksen, T. E.: pH Effects on the pulse radiolysis of deoxygenated aqueous solutions of sulphur dioxide, Journal of the Chemical Society, Faraday Transactions 1: Physical Chemistry in Condensed Phases, 70, 208-215, 10.1039/f19747000208, 1974.

Gao, M., Carmichael, G. R., Wang, Y., Ji, D., Liu, Z., and Wang, Z.: Improving simulations of sulfate aerosols during winter haze over Northern China: the impacts of heterogeneous oxidation by NO2, Front. Environ. Sci. Eng., 10, 16, 10.1007/s11783-016-0878-2, 2016.

Guo, H., Weber, R. J., and Nenes, A.: High levels of ammonia do not raise fine particle pH sufficiently to yield nitrogen oxide-dominated sulfate production, Sci. Rep., 7, 12109, 10.1038/s41598-017-11704-0, 2017.

Hayon, E., Treinin, A., and Wilf, J.: Electronic spectra, photochemistry, and autoxidation mechanism of the sulfite-bisulfite-pyrosulfite systems. SO2-, SO3-, SO4-, and SO5- radicals, J. Am. Chem. Soc. , 94, 47-57, 10.1021/ja00756a009, 1972.

He, H., Wang, Y., Ma, Q., Ma, J., Chu, B., Ji, D., Tang, G., Liu, C., Zhang, H., and Hao, J.: Mineral dust and NOx promote the conversion of SO2 to sulfate in heavy pollution days, Sci. Rep., 4, 10.1038/srep04172, 2014.

Herrmann, H.: Kinetics of aqueous phase reactions relevant for atmospheric chemistry, Chem. Rev., 103, 4691-4716, 10.1021/cr020658q, 2003.

Herrmann, H., Schaefer, T., Tilgner, A., Styler, S. A., Weller, C., Teich, M., and Otto, T.: Tropospheric Aqueous-Phase Chemistry: Kinetics, Mechanisms, and Its Coupling to a Changing Gas Phase, Chem. Rev., 115, 4259-4334, 10.1021/cr500447k, 2015.

Huang, L., Zhao, Y., Li, H., and Chen, Z.: Kinetics of Heterogeneous Reaction of Sulfur Dioxide on Authentic Mineral Dust: Effects of Relative Humidity and Hydrogen Peroxide, Environ. Sci. Technol., 49, 10797-10805, 10.1021/acs.est.5b03930, 2015.

Huie, R. E., and Neta, P.: Kinetics of one-electron transfer-reactions involving ClO2 and NO2, J. Phys. Chem. , 90, 1193-1198, 10.1021/j100278a046, 1986.
Huie, R. E., and Neta, P.: Rate constants for some oxidations of S(IV) by radicals in aqueous-solutions, Atmos. Environ., 21, 1743-1747, 10.1016/0004-6981(87)90113-2, 1987.
Huie, R. E., Clifton, C. L., and Altstein, N.: A pulse radiolysis and flash photolysis study of the radicals SO2, SO3, SO4 and SO5, Radiat. Phys. Chem. , 33, 361-370, 1989.
Huie, R. E.: Free radical chemistry of the atmospheric aqueous phase, in: Progress and Problems in Atmospheric Chemistry, WORLD SCIENTIFIC, 374-419, 1995.
Lee, Y.-N., and Schwartz, S. E.: Kinetics of oxidation of aqueous sulfur (IV) by nitrogen dioxide, in: Precipitation Scavenging, Dry Deposition and Resuspension, edited by: Pruppacher, H. R., Semonin, R. G., and Slinn, W. G. N., Elsevier, New York, 453-466, 1983.
Lelieveld, J., Gromov, S., Pozzer, A., and Taraborrelli, D.: Global tropospheric hydroxyl distribution, budget and reactivity, Atmos. Chem. Phys., 16, 12477-12493, 10.5194/acp-16-12477-2016, 2016.
Li, H. J., Zhu, T., Zhao, D. F., Zhang, Z. F., and Chen, Z. M.: Kinetics and mechanisms of heterogeneous reaction of NO_2 on $CaCO_3$ surfaces under dry and wet conditions, Atmos. Chem. Phys., 10, 463-474, 2010.
Littlejohn, D., Wang, Y. Z., and Chang, S. G.: Oxidation of aqueous sulfite ion by nitrogen-dioxide, Environ. Sci. Technol., 27, 2162-2167, 10.1021/es00047a024, 1993.
Liu, M. X., Song, Y., Zhou, T., Xu, Z. Y., Yan, C. Q., Zheng, M., Wu, Z. J., Hu, M., Wu, Y. S., and Zhu, T.: Fine particle pH during severe haze episodes in northern China, Geophys. Res. Lett., 44, 5213-5221, 10.1002/2017gl073210, 2017.
Liu, Y. J., Zhu, T., Zhao, D. F., and Zhang, Z. F.: Investigation of the hygroscopic properties of Ca(NO3)(2) and internally mixed Ca(NO3)(2)/CaCO3 particles by micro-Raman spectrometry, Atmos. Chem. Phys., 8, 7205-7215, 2008.
Ma, Q., He, H., Liu, Y., Liu, C., and Grassian, V. H.: Heterogeneous and multiphase formation pathways of gypsum in the atmosphere, Phys. Chem. Chem. Phys., 15, 19196-19204, 10.1039/c3cp53424c, 2013.
Nakamoto, K.: Infrared and Raman Spectra of Inorganic and Coordination Compounds Part A, John Wiley &Sons, New York, 221-247 pp., 1997.
Nash, T.: Effect of nitrogen-dioxide and of some transition-metals on the oxidation of dilute bisulfite solutions, Atmos. Environ., 13, 1149-1154, 10.1016/0004-6981(79)90038-6, 1979.
Pöschl, U., Rudich, Y., and Ammann, M.: Kinetic model framework for aerosol and cloud surface chemistry and gas-particle interactions - Part 1: General equations, parameters, and terminology, Atmos. Chem. Phys., 7, 5989-6023, 2007.
Podkrajšek, B., Grgić, I., and Turšič, J.: Determination of sulfur oxides formed during the S(IV) oxidation in the presence of iron, Chemosphere, 49, 271-277, https://doi.org/10.1016/S0045-6535(02)00324-7, 2002.
Prinn, R. G., Huang, J., Weiss, R. F., Cunnold, D. M., Fraser, P. J., Simmonds, P. G., McCulloch, A., Harth, C., Reimann, S., Salameh, P., O'Doherty, S., Wang, R. H. J., Porter, L. W., Miller, B. R., and Krummel, P. B.: Evidence for variability of atmospheric hydroxyl radicals over the past quarter century, Geophys. Res. Lett., 32, 10.1029/2004gl022228, 2005.

Santachiara, G., Prodi, F., and Vivarelli, F.: SO2 oxidation in monodisperse droplets grown on carbon nuclei in presence of NO2, J. Aerosol Sci., 21, S221-S224, 10.1016/0021-8502(90)90224-l, 1990.

Santachiara, G., Prodi, F., and Vivarelli, F.: Further experiments on SO2 oxidation rate in monodisperse droplets grown on carbon nuclei in presence of O-2 and NO2, J. Aerosol Sci., 24, 683-685, 10.1016/0021-8502(93)90024-4, 1993.

Sarma, L. P., Prasad, P. S. R., and Ravikumar, N.: Raman spectroscopic study of phase transitions in natural gypsum, J. Raman Spectrosc. , 29, 851-856, 10.1002/(sici)1097-4555(199809)29:9<851::aid-jrs313>3.0.co;2-s, 1998.

Seinfeld, J. H., and Pandis, S. N.: Atmospheric chemistry and physics: from air pollution to climate change, 2nd ed., John Wiley &Sons. Inc., 2006.

Shen, C. H., and Rochelle, G. T.: Nitrogen Dioxide Absorption and Sulfite Oxidation in Aqueous Sulfite, Environ. Sci. Technol., 32, 1994-2003, 10.1021/es970466q, 1998.

Shi, X. L.: Generation of SO_3^- and OH radicals in SO_3^{2-} reactions with inorganic environmental-pollutants and its implications to SO_3^{2-} toxicity, J. Inorg. Biochem. , 56, 155-165, 10.1016/0162-0134(94)85002-x, 1994.

Spindler, G., Hesper, J., Bruggemann, E., Dubois, R., Muller, T., and Herrmann, H.: Wet annular denuder measurements of nitrous acid: laboratory study of the artefact reaction of NO2 with S(IV) in aqueous solution and comparison with field measurements, Atmos. Environ., 37, 2643-2662, 10.1016/s1352-2310(03)00209-7, 2003.

Turšič, J., Grgić, I., and Bizjak, M.: Influence of NO2 and dissolved iron on the S(IV) oxidation in synthetic aqueous solution, Atmos. Environ., 35, 97-104, https://doi.org/10.1016/S1352-2310(00)00283-1, 2001.

Wang, G., Zhang, R., Gomez, M. E., Yang, L., Levy Zamora, M., Hu, M., Lin, Y., Peng, J., Guo, S., Meng, J., Li, J., Cheng, C., Hu, T., Ren, Y., Wang, Y., Gao, J., Cao, J., An, Z., Zhou, W., Li, G., Wang, J., Tian, P., Marrero-Ortiz, W., Secrest, J., Du, Z., Zheng, J., Shang, D., Zeng, L., Shao, M., Wang, W., Huang, Y., Wang, Y., Zhu, Y., Li, Y., Hu, J., Pan, B., Cai, L., Cheng, Y., Ji, Y., Zhang, F., Rosenfeld, D., Liss, P. S., Duce, R. A., Kolb, C. E., and Molina, M. J.: Persistent sulfate formation from London Fog to Chinese haze, Proc. Nat. Acad. Sci. U.S.A., 113, 13630-13635, 10.1073/pnas.1616540113, 2016.

Waygood, S. J., and McElroy, W. J.: Spectroscopy and decay kinetics of the sulfite radical anion in aqueous solution, J. Chem. Soc.-Faraday Trans., 88, 1525-1530, 10.1039/ft9928801525, 1992.

Xue, J., Yuan, Z. B., Griffith, S. M., Yu, X., Lau, A. K. H., and Yu, J. Z.: Sulfate Formation Enhanced by a Cocktail of High NOx, SO2, Particulate Matter, and Droplet pH during Haze-Fog Events in Megacities in China: An Observation-Based Modeling Investigation, Environ. Sci. Technol., 50, 7325-7334, 10.1021/acs.est.6b00768, 2016.

Zhang, J. K., Sun, Y., Liu, Z. R., Ji, D. S., Hu, B., Liu, Q., and Wang, Y. S.: Characterization of submicron aerosols during a month of serious pollution in Beijing, 2013, Atmos. Chem. Phys., 14, 2887-2903, 10.5194/acp-14-2887-2014, 2014.

Zhao, D., Song, X., Zhu, T., Zhang, Z., and Liu, Y.: Multiphase Reaction of SO2 with NO2 on CaCO3 Particles. 1. Oxidation of SO2 by NO2, Atmos. Chem. Phys. Discuss., 2017, 1-23, 10.5194/acp-2017-610, 2017.

Zhao, D. F., Zhu, T., Chen, Q., Liu, Y. J., and Zhang, Z. F.: Raman micro-spectrometry as a technique for investigating heterogeneous reactions on individual atmospheric particles, Sci. China Chem., 54, 154-160, 10.1007/s11426-010-4182-x, 2011.

Zheng, B., Zhang, Q., Zhang, Y., He, K. B., Wang, K., Zheng, G. J., Duan, F. K., Ma, Y. L., and Kimoto, T.: Heterogeneous chemistry: a mechanism missing in current models to explain secondary inorganic aerosol formation during the January 2013 haze episode in North China, Atmos. Chem. Phys., 15, 2031-2049, 10.5194/acp-15-2031-2015, 2015a.

Zheng, G. J., Duan, F. K., Su, H., Ma, Y. L., Cheng, Y., Zheng, B., Zhang, Q., Huang, T., Kimoto, T., Chang, D., Poschl, U., Cheng, Y. F., and He, K. B.: Exploring the severe winter haze in Beijing: the impact of synoptic weather, regional transport and heterogeneous reactions, Atmos. Chem. Phys., 15, 2969-2983, 10.5194/acp-15-2969-2015, 2015b.

Zhu, T., Shang, J., and Zhao, D. F.: The roles of heterogeneous chemical processes in the formation of an air pollution complex and gray haze, Sci. China Chem., 54, 145-153, 10.1007/s11426-010-4181-y, 2011.

Table 1. Reactive uptake coefficient of SO_2 for sulfate formation at 82% RH and at different O_2 concentrations.

SO_2/NO_2/O_2 concentration	**γ**
75 ppm/ 75 ppm/ 86 %	1.7×10^{-5}
75 ppm/ 75 ppm/ 20 %	1.2×10^{-5}
75 ppm/ 75 ppm/ 5 %	3.5×10^{-6}

489 **Table 2.** Summary of the mechanism of the reaction S(IV) with O_2/NO_2

Step	Reactions	
Initiation	$NO_2(aq) + HSO_3^-(aq) \rightarrow NO_2^-(aq) + SO_3^{\bullet-}(aq) + H^+(aq)$	(R8)
Propagation	$SO_3^{\bullet-}(aq) + O_2(aq) \rightarrow SO_5^{\bullet-}(aq)$	(R12)
	$SO_5^{\bullet-}(aq) + HSO_3^-(aq) \rightarrow HSO_5^-(aq) + SO_3^{\bullet-}(aq)$	(R13)
	$HSO_5^-(aq) + HSO_3^-(aq) \rightarrow 2SO_4^{2-}(aq) + 2H^+(aq)$	(R14)
	$SO_5^{\bullet-}(aq) + HSO_3^-(aq) \rightarrow SO_4^{2-}(aq) + SO_4^{\bullet-}(aq) + H^+(aq)$	(R15)
	$SO_4^{\bullet-}(aq) + HSO_3^-(aq) \rightarrow SO_4^{2-}(aq) + SO_3^{\bullet-}(aq) + H^+(aq)$	(R16)
Termination	$SO_3^{\bullet-}(aq) + SO_3^{\bullet-}(aq) \rightarrow S_2O_6^{2-}(aq)$	(R9)
	$SO_3^{\bullet-}(aq) + SO_3^{\bullet-}(aq) \rightarrow SO_3^{2-}(aq) + SO_3$	(R10)
	$SO_3(aq) + H_2O \rightarrow SO_4^{2-}(aq) + 2H^+(aq)$	(R11)
	$SO_4^{\bullet-}(aq) + SO_4^{\bullet-}(aq) \rightarrow S_2O_8^{2-}(aq)$	(R17)
	$SO_5^{\bullet-}(aq) + SO_5^{\bullet-}(aq) \rightarrow S_2O_8^{2-}(aq) + O_2(aq)$	(R18)

490

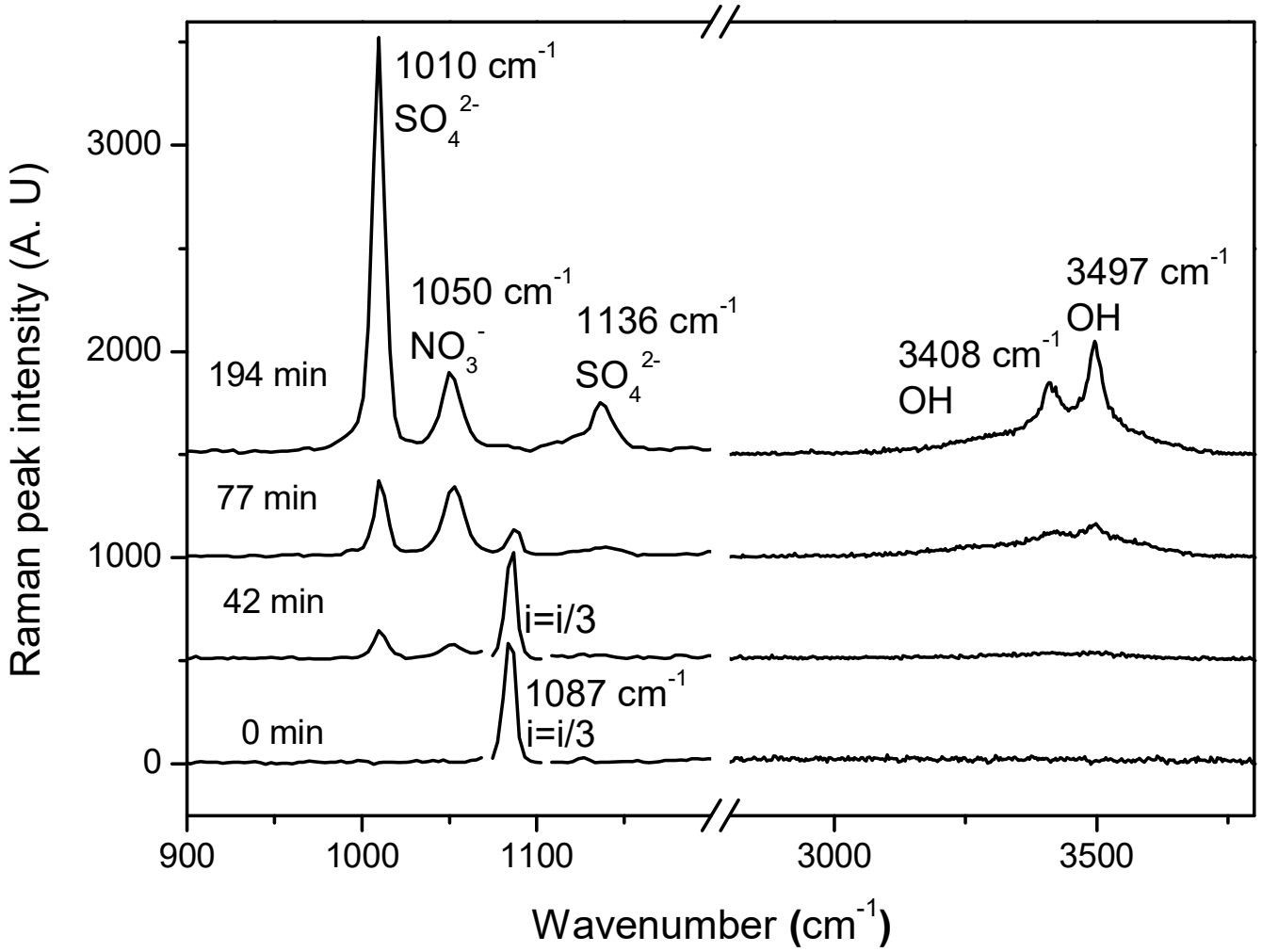

491

492 Figure 1. Raman spectra of a $CaCO_3$ particle during the multiphase reaction of SO_2 with $O_2/NO_2/H_2O$
493 on the particle. SO_2: 75 ppm, NO_2: 75 ppm, RH: 72%, O_2: 20%. The peak intensity of carbonate (1087
494 cm^{-1}) at 0 and 42 min was divided by three for clarity.

495

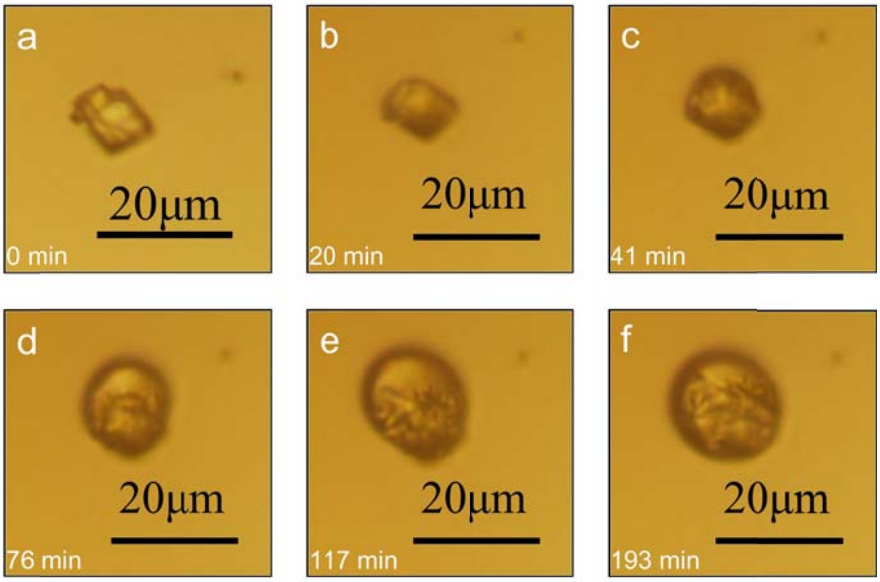
a
20μm
0 min
b
20μm
20 min
c
20μm
41 min
d
20μm
76 min
e
20μm
117 min
f
20μm
193 min

(i)

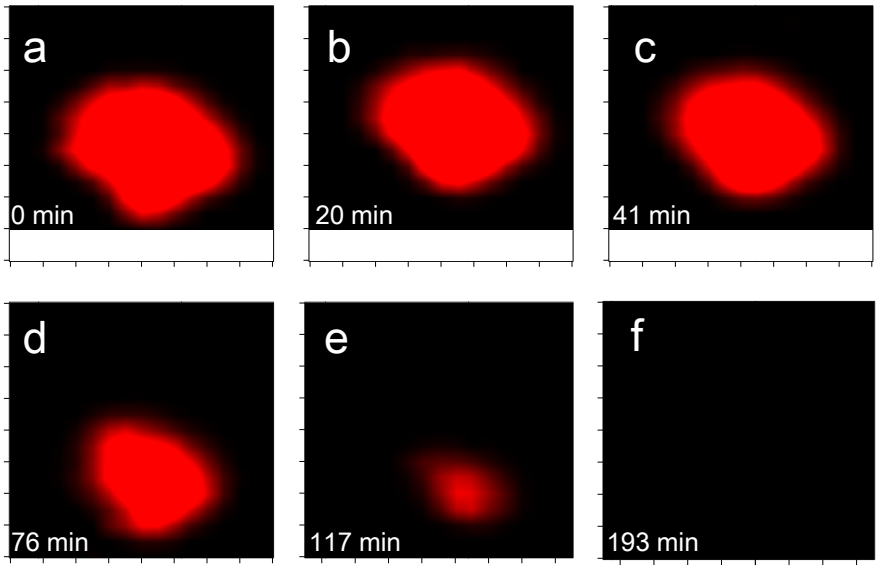
a
0 min
b
20 min
c
41 min
d
76 min
e
117 min
f
193 min

(ii)

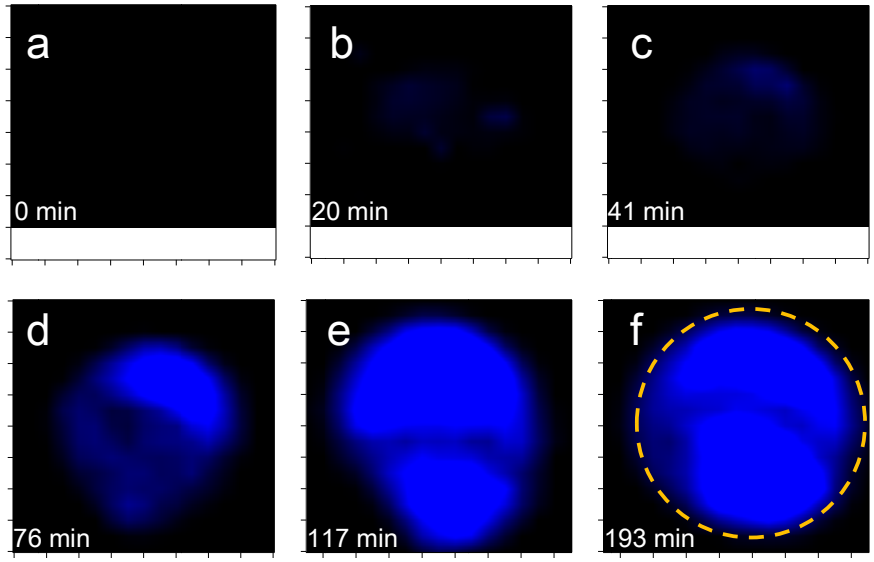
a
0 min
b
20 min
c
41 min
d
76 min
e
117 min
f
193 min

(iii)

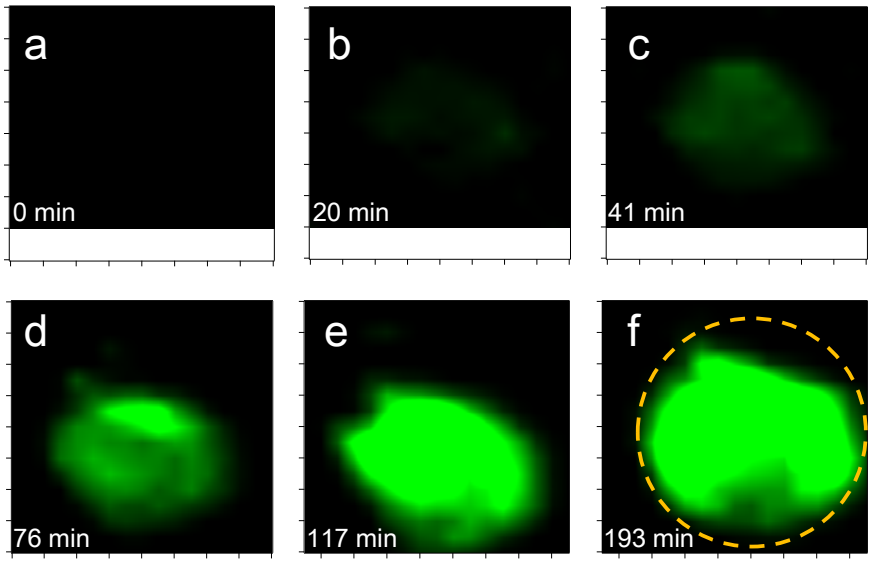

(iv)

Figure 2. Microscopic image (i) and Raman mapping image of carbonate (ii), nitrate (iii), and sulfate (iv) on the $CaCO_3$ particle during the multiphase reaction SO_2 with $O_2/NO_2/H_2O$ on the particle. A-f corresponds to the reaction time of 0, 20, 41, 76, 117, and 193 min. SO_2: 75 ppm, NO_2: 75 ppm, RH: 72%, O_2: 20%. The mapping image of carbonate, nitrate, and sulfate are made using the peak area at 1050, 1010, and 1087 cm^{-1}, respectively. The red, blue, and green colors indicate the peak intensity of carbonate, nitrate, and sulfate, respectively. The dashed lines in panel iii-f and iv-f indicate the shape of the droplet at the end of the reaction.

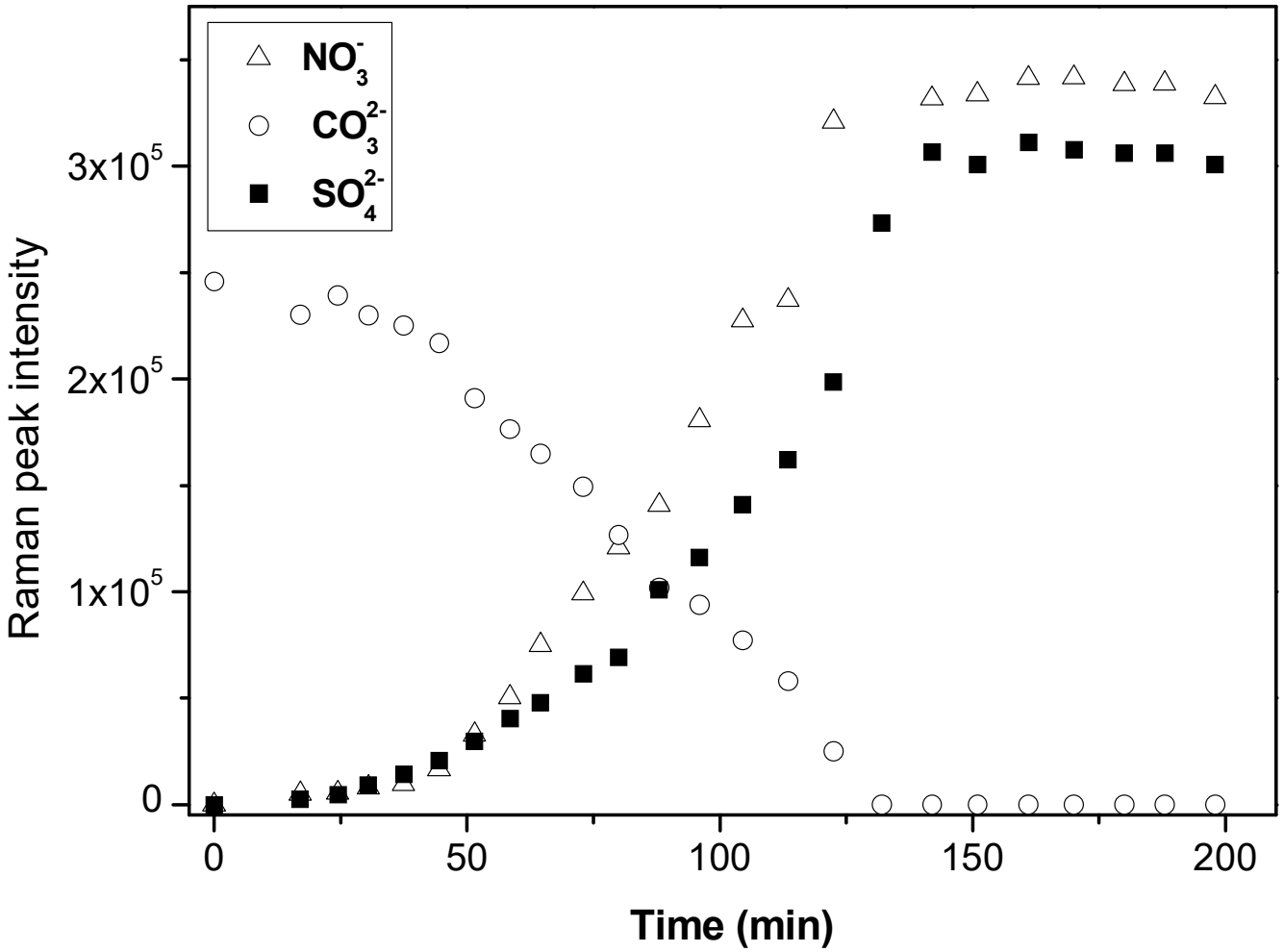

Figure 3. Time series of the Raman peak intensity of NO_3^-, SO_4^{2-}, and CO_3^{2-} during the reaction of SO_2 with $O_2/NO_2/H_2O$ on $CaCO_3$ particles. SO_2: 75 ppm, NO_2: 75 ppm, RH: 72%, O_2: 20%. The intensity of NO_3^-, SO_4^{2-}, and CO_3^{2-} show the peak area at 1050, 1010, and 1087 cm^{-1}, respectively, in Raman spectra obtained by Raman mapping.